ARTICLES

Simulation algorithms for multidimensional nonlinear response of classical many-body systems

Christoph Dellago
Institute for Experimental Physics, University of Vienna, Boltzmanngasse 5, A-1090 Vienna, Austria

Shaul Mukamel
Department of Chemistry, University of California, Irvine, California 92697-2025

(Received 14 July 2003; accepted 15 August 2003)

The numerical effort and convergence of equilibrium and nonequilibrium (finite field) techniques for simulating the response of classical systems to a sequence of n short pulses are examined. The former is recast in terms of n point correlation functions and nth order stability matrices which contain higher order generalized Lyapunov exponents, whereas the latter involves sums over perturbed trajectories. The two methods are tested for a highly chaotic system: The Lorentz gas, and for the less chaotic quartic oscillator. © *2003 American Institute of Physics.*
[DOI: 10.1063/1.1616911]

I. INTRODUCTION

Dynamical systems may be effectively studied by subjecting them to external perturbations and watching the response.[1–3] Most valuable information may be extracted from *multidimensional techniques*[4–6] based on the application of a sequence of n short pulses at time $\tau_1,\ldots,\tau_n$ and measuring a signal after the last pulse at time $t>\tau_n$. Coherent NMR and laser spectroscopy provide snapshots of spins, vibrational and electronic dynamics over a broad range of timescales from femtoseconds to milliseconds.[7] Recently, higher order Raman spectroscopy has received much attention.[8–11] Other types of perturbations (mechanical, temperature jump, voltage) are widely used as well.

Denoting the external field envelope by $E(\tau)$, the signal can most generally be expressed as the expectation value of a dynamical variable B at the time of measurement t. To nth order in the field we have

$$B^{(n)}(t)=\int_0^t d\tau_n\int_0^{\tau_n} d\tau_{n-1}\cdots\int_0^{\tau_2} d\tau_1 E(\tau_n)E(\tau_{n-1})\cdots E(\tau_2)\times E(\tau_1)S^{(n)}(t,\tau_n,\tau_{n-1}\ldots,\tau_2,\tau_1). \quad (1)$$

Here, $S^{(n)}(t,\tau_n,\tau_{n-1},\ldots,\tau_2,\tau_1)$ is the nth order *response function* of the system. The variation of the response with the n time intervals $\tau_{j+1}-\tau_j$ with $j=1,...,n$ (where we set $t=\tau_{n+1}$) provides n-dimensional (nD) correlation plots, from which details on the system's dynamics can be extracted. The same information may be obtained in the frequency domain by using long continuous-wave (CW) perturbing fields and tuning their frequencies. The connection between the two in terms of multidimensional Fourier transforms is well documented and will not be discussed here.[5]

In this paper we examine two basic strategies for determining classical nonlinear response functions (NRFs) with computer simulations: equilibrium (correlation function)[12,13] and nonequilibrium (finite field)[14] simulations. The former is based on unperturbed trajectories of the system with no external force; the same trajectories can then generate the response for all values of $\tau_1,\ldots,\tau_n$. This is a notable advantage. On the other hand, the simulations are complicated by the appearance of stability matrices which diverge rapidly with time. This poses a severe limitation on the accuracy and limits practical simulations to short times. In nonequilibrium simulations, on the other hand, the trajectories are run and are perturbed at the times of interactions with the fields. No numerically problematic stability matrices appear. However, the simulation requires different trajectories for each choice of $\tau_1,\ldots,\tau_n$ and therefore needs to be repeated many times. We shall survey both strategies and propose new equilibrium simulation techniques without stability matrices which will combine the advantages of both methods.

II. EQUILIBRIUM "SCHRÖDINGER PICTURE" REPRESENTATION

We consider a system with Hamiltonian $H_0(x)$ coupled to a spatially homogeneous field $E(t)$ through

$$H'(x,t)=-E(t)A(x), \quad (2)$$

where x is a point in phase-space (coordinates and momenta) and $A(x)$ is an arbitrary phase-space variable, such as the dipole moment of the system. The total Hamiltonian of the externally driven system is

$$H(x,t)=H_0(x)+H'(x,t). \quad (3)$$

The phase-space density $\rho(x,t)$ evolves according to the Liouville equation,

$$\frac{\partial\rho}{\partial t}=-iL\rho, \quad iL=\{\ldots,H\}=\{\ldots,H_0+H'\}=iL_0+iL'. \quad (4)$$

Here, {..., ...} is the classical *Poisson bracket* which for two arbitrary phase-space variable $A(x)$ and $B(x)$ reads

$$\{A,B\}=\omega_{ij}\frac{\partial A}{\partial x_i}\frac{\partial B}{\partial x_j}. \quad (5)$$

Here and in the following Einstein's summation convention is implied and ω_{ij} takes values -1, 0, and 1.

We now expand $\rho(x,t)$ in powers of the strength of the external field,

$$\rho(x,t)=\rho^{(0)}(x,t)+\rho^{(1)}(x,t)+\cdots+\rho^{(n)}(x,t)+\cdots. \quad (6)$$

The zeroth order term $\rho^{(0)}(x,t)$ is the unperturbed phase-space density and we assume that it is an equilibrium distribution conserved by the phase flow with Liouville operator L_0, i.e., $\rho^{(0)}(x,t)=\rho_{\mathrm{equ}}(x)$.

Inserting Eq. (6) into the Liouville equation (4) and collecting terms of the same order one obtains a set of coupled differential equations. These equations can be formally solved yielding[15,16]

$$\rho^{(1)}(t)=\int_0^t d\tau_1 e^{-iL_0(t-\tau_1)}\{H',\rho_{\mathrm{equ}}\}, \quad (7)$$

$$\rho^{(2)}(t)=\int_0^t d\tau_2\int_0^{\tau_2} d\tau_1 e^{-iL_0(t-\tau_2)}\{H',e^{-iL_0(\tau_2-\tau_1)}\times\{H',\rho_{\mathrm{equ}}\}\}, \quad (8)$$

$$\cdots$$

$$\rho^{(n)}(t)=\int_0^t d\tau_n\int_0^{\tau_n} d\tau_{n-1}\cdots\int_0^{\tau_2} d\tau_1 e^{-iL_0(t-\tau_n)}\times\{H',e^{-iL_0(\tau_n-\tau_{n-1})}\{H',\ldots\{H',e^{-iL_0(\tau_2-\tau_1)}\times\{H',\rho_{\mathrm{equ}}\}\}\cdots\}\}, \quad (9)$$

where we have assumed that the system is in equilibrium prior to $t=0$.

The time dependent average of an observable $B(x(t))$ is

$$\langle B(t)\rangle=\int dx\rho(x,t)B(x). \quad (10)$$

The integration in the above equation extends over the entire phase-space. Using the expansion for the phase-space density $\rho(x,t)$ we can separate the different orders in the external field,

$$B^{(n)}(t)\equiv\int dx\rho^{(n)}(x,t)B(x). \quad (11)$$

Thus, for perturbations of type (2) the response functions from Eq. (1) are

$$S^{(n)}(t,\tau_n,\tau_{n-1},\ldots,\tau_2,\tau_1)=(-1)^n\int dxB(x)e^{-iL_0(t-\tau_n)}\times\{A,e^{-iL_0(\tau_n-\tau_{n-1})}\times\{\ldots,e^{-iL_0(\tau_2-\tau_1)}\{A,\rho_{\mathrm{equ}}\}\}\cdots\}. \quad (12)$$

This nth order NRF describing the response at time t to n short pulses at times $\tau_1,\ldots,\tau_n$ can be recast in the following compact form:[5]

$$S^{(n)}(t,\tau_n,\tau_{n-1},\ldots,\tau_2,\tau_1)=\langle\langle B|\mathcal{G}(t-\tau_n)\cdots\tilde{A}\mathcal{G}(\tau_2-\tau_1)\tilde{A}|\rho_{\mathrm{equ}}\rangle\rangle. \quad (13)$$

Here, $\tilde{A}B\equiv\{A,B\}$ is the Poisson bracket for two arbitrary phase-space variables $A(x)$ and $B(x)$. The double bracket $\langle\langle\cdots\rangle\rangle$ denotes a matrix element in Liouville space. Equation (13) can be interpreted as follows: We start with the equilibrium phase-space distribution which is a vector in Liouville space denoted by the ket $|\rho_{\mathrm{equ}}\rangle\rangle$. Each of the n actions of the external field on the distribution is represented by a Poisson bracket $\tilde{A}$. In the time intervals between actions the time evolution is described by $\mathcal{G}(\tau)\equiv\exp(-iL\tau)$, where $L=\tilde{H}$ is the Liouville operator. Both $\tilde{A}$ and $\mathcal{G}(\tau)$ are operators in Liouville space. Finally we multiply the evolved distribution with the bra $\langle\langle B|$ and take the trace. This yields the change in the expectation value of B to nth order in the field for impulsive (very short) fields. The response to arbitrary field envelopes can then be obtained from Eq. (1).

To evaluate the response function $S^{(n)}$ we use the identity

$$\{A,\rho\}=-\beta\dot{A}\rho, \quad (14)$$

for a canonical equilibrium distribution ρ. The first order response is then given by

$$S^{(1)}(t,\tau_1)=\frac{d}{d\tau_1}\beta\langle B(t)A(\tau_1)\rangle. \quad (15)$$

This *fluctuation dissipation theorem*[17] connects the observable linear response function $S^{(1)}$ with an equilibrium correlation function of the unperturbed system. In order to compute higher order NRFs we introduce a hierarchy of different order stability matrices defined as follows:

$$M_i^{(0)}(\tau_1)\equiv x_i(\tau_1), \quad (16)$$

$$M_{ij}^{(1)}(\tau_2,\tau_1)\equiv\frac{\partial x_j(\tau_1)}{\partial x_i(\tau_2)}, \quad (17)$$

$$M_{ijk}^{(2)}(\tau_3,\tau_2,\tau_1)\equiv\frac{\partial^2 x_k(\tau_1)}{\partial x_i(\tau_3)\partial x_j(\tau_2)}, \quad (18)$$

and so on. The $(n+1)$-time nth order stability matrix is generally defined as

$$M_{i_{n+1},\ldots,i_1}^{(n)}(\tau_{n+1},\tau_n,\ldots,\tau_2,\tau_1)\equiv\frac{\partial^n x_{i_1}(\tau_1)}{\partial x_{i_{n+1}}(\tau_{n+1})\cdots\partial x_{i_2}(\tau_2)}. \quad (19)$$

$M_{jk}^{(1)}(\tau_2,\tau_1)$ is the *stability* (or *monodromy) matrix* associated with the dynamics. Using this notation, the second order response can be written as

$$S^{(2)}(t,\tau_2,\tau_1)=\beta^2\frac{d^2}{d\tau_1 d\tau_2}\langle B(t)A(\tau_2)A(\tau_1)\rangle-\beta\frac{d}{d\tau_1}\langle B(t)\omega_{ij}\times M_{jk}^{(1)}(\tau_2,\tau_1)A_i'(\tau_2)A_k'(\tau_1)\rangle, \quad (20)$$

where $A_i'\equiv\partial A/\partial x_i$. The third order response assumes the form

$$S^{(3)}(t,\tau_3,\tau_2,\tau_1)=\beta^3\frac{d^3}{d\tau_1 d\tau_2 d\tau_3}\langle B(t)A(\tau_3)A(\tau_2)A(\tau_1)\rangle-\beta^2\frac{d^2}{d\tau_1 d\tau_2}\langle B(t)\omega_{ij}A_i'(\tau_3)A_k'(\tau_2)A(\tau_1)M_{jk}^{(1)}(\tau_3,\tau_2)\rangle$$
$$-\beta^2\frac{d^2}{d\tau_1 d\tau_2}\langle B(t)\omega_{ij}A_i'(\tau_3)A_k'(\tau_1)A(\tau_2)M_{jk}^{(1)}(\tau_3,\tau_1)\rangle$$
$$-\beta^2\frac{d^2}{d\tau_1 d\tau_3}\langle B(t)\omega_{ij}A_i'(\tau_2)A_k'(\tau_1)A(\tau_3)M_{jk}^{(1)}(\tau_2,\tau_1)\rangle$$
$$+\beta\frac{d}{d\tau_1}\langle B(t)\omega_{mn}\omega_{ij}A_m'(\tau_3)A_{il}''(\tau_2)A_k'(\tau_1)M_{nl}^{(1)}(\tau_3,\tau_2)M_{jk}^{(1)}(\tau_2,\tau_1)\rangle$$
$$+\beta\frac{d}{d\tau_1}\langle B(t)\omega_{mn}\omega_{ij}A_m'(\tau_3)A_i'(\tau_2)A_{kl}''(\tau_1)M_{nl}^{(1)}(\tau_3,\tau_1)M_{jk}^{(1)}(\tau_2,\tau_1)\rangle$$
$$+\beta\frac{d}{d\tau_1}\langle B(t)\omega_{mn}\omega_{ij}A_m'(\tau_3)A_i'(\tau_2)A_k'(\tau_1)M_{ljk}^{(2)}(\tau_2,\tau_2,\tau_1)M_{nl}^{(1)}(\tau_3,\tau_2)\rangle. \quad (21)$$

Here, $A_{kl}''(x)\equiv\partial^2 A(x)/\partial x_k\partial x_l$. Note that in Eq. (11) of Ref. 12, $M^{(2)}$ has been factorized. Equation (21) is the complete expression for the third order response function. While the linear response can be written as a simple correlation function, expressions for the second and third order response involve first and second order stability matrices, respectively. In general, nth order response functions involve stability matrices up to order $n-1$.

In a practical calculation stability matrices can be determined by integration of appropriate equations of motion. For instance, application of the chain rule yields an equation of motion for the first order stability matrix,

$$\frac{d}{dt'}M_{jk}^{(1)}(t,t')=M_{ji}^{(1)}(t,t')\frac{\partial\dot{x}_k(t')}{\partial x_j(t')}. \quad (22)$$

The derivatives $\partial\dot{x}_k(t')/\partial x_j(t')$ appearing in the right-hand side of the above equation involve second derivatives of the potential energy. This equation of motion can be solved with the same integrator used to determine the time evolution of the system itself. For high order stability matrices similar equations of motion can be derived.

So far we have considered a canonical ensemble. Equations (14) can be extended for any ρ which is a function of the Hamiltonian only,

$$\{A,\rho[H(x)]\}=\{A,H\}\frac{\partial\rho}{\partial H}=\dot{A}\frac{\partial\rho}{\partial H}. \quad (23)$$

In particular, in the microcanonical ensemble $\rho[H(x)]\propto\delta(E-H)$ we have $\{A,\rho(H)\}=\dot{A}\partial\rho/\partial E$. Expressions for canonical response functions can therefore be easily modified to a microcanonical ensemble by using microcanonical correlation functions and simply replacing β by $\partial/\partial E$. For instance, the microcanonical fluctuation dissipation theorem reads

$$S_{\mathrm{mc}}^{(1)}=-\frac{\partial}{\partial E}\frac{\partial}{\partial\tau_1}\langle B(t)A(\tau_1)\rangle_{\mathrm{mc}}. \quad (24)$$

III. "HEISENBERG" AND INTERMEDIATE EQUILIBRIUM REPRESENTATIONS OF RESPONSE FUNCTIONS

By invoking the classical analogues of the Schrödinger and Heisenberg pictures we can recast Eq. (13) in different forms, which provide complementary insights. In the previous section we let the Poisson brackets in Eq. (13) act to the right. This is the classical analogue of the *Schrödinger picture* whereby the phase-space density changes with time. Time dependent averages $\langle B(t)\rangle$ are then written over this evolving phase-space density $\rho(x,t)$ [see Eq. (10)]. Alternatively, $S^{(n)}$ can be evaluated by acting with all Poisson brackets to the left. Using this *Heisenberg picture* (operators, rather than the density matrix, change with time) we find that $S^{(n)}$ can be written in terms of an $(n+1)$-time nth order stability matrix. This alternative view considers the time evolution of observables along trajectories starting from phase-space points distributed according to an initial phase-space density,

$$\langle B(t)\rangle=\int dx\rho(x,0)B[x(t)]. \quad (25)$$

In the Heisenberg picture, dynamical variables $B[x(t)]$ evolve according to the Liouville equation

$$\frac{\partial B}{\partial t}=iLB, \quad (26)$$

where L is the Liouville operator from Eq. (4).

By repeated integration by parts using

$$\int dxA\{B,C\}=\int dx\{A,B\}C, \quad (27)$$

one can move from the Schrödinger picture to the Heisenberg picture of nonlinear response functions. Integrating by parts once and using $B(t)=\exp(iLt)B(0)$ we obtain the first order response function in the Heisenberg picture,

$$S^{(1)}(t,\tau_1)=\langle\{A(\tau_1),B(t)\}\rangle. \quad (28)$$

The second order response function is

$$S^{(2)}(t,\tau_2,\tau_1)=\langle\{A(\tau_1),\{A(\tau_2),B(t)\}\}\rangle, \tag{29}$$

and the nth order response function can be written very compactly as

$$S^{(n)}(t,\tau_n,\ldots,\tau_1) =\langle\{A(\tau_1),\{A(\tau_2),\ldots\{A(\tau_{n-1}),\{A(\tau_n),B(t)\}\}\cdots\}\}\rangle. \tag{30}$$

Note that the double bracket expression [Eq. (13)] includes both representations.

Evaluating the Poisson brackets appearing in the Heisenberg form of the response functions becomes complicated rapidly with growing order. The first and second order response functions obtained from the above expressions are

$$S^{(1)}(t,\tau_1)=\langle\omega_{ij}A_i'(\tau_1)B_k'(t)M_{jk}^{(1)}(\tau_1,t)\rangle, \tag{31}$$

and

$$\begin{aligned}S^{(2)}(t,\tau_2,\tau_1)=\langle\omega_{ij}\omega_{kl}A_i'(\tau_1)[&A_{mr}''(\tau_2)M_{jr}^{(1)}(\tau_1,\tau_2)\\ &\times M_{km}^{(1)}(\tau_1,\tau_2)B_n'(t)M_{ln}^{(1)}(\tau_1,t)+A_m'(\tau_2)\\ &\times M_{jkm}^{(2)}(\tau_1,\tau_1,\tau_2)B_n'(t)M_{ln}^{(1)}(\tau_1,t)+A_m'(\tau_2)\\ &\times M_{km}^{(1)}(\tau_1,\tau_2)B_{ns}''(t)M_{js}^{(1)}(\tau_1,t)M_{ln}^{(1)}(\tau_1,t)\\ &+A_m'(\tau_2)M_{km}^{(1)}(\tau_1,\tau_2)B_n'(t)M_{ljn}^{(2)}(\tau_1,\tau_1,t)]\rangle.\end{aligned} \tag{32}$$

The third order response can be worked out, but it is rather complicated and is omitted here. Note that a first order stability matrix appears in the linear response and that the second order response depends on stability matrices up to order two. In general, $S^{(n)}$ explicitly depends on stability matrices up to $M^{(n)}$ and may not be written in terms of simple correlation functions alone. While in the Heisenberg picture the highest stability matrix degree appearing in the expressions of nth order NRFs is n, it is only $(n-1)$ in the Schrödinger picture.

For nth order n integrations by part are necessary to go all the way from Schrödinger to Heisenberg representation. But these two pictures are not the only possible ones. For nth order there are a total of $n+1$ different ways to distribute the time dependence between the observables and the phase-space density. Equation (13) has n $\tilde{A}$ factors. The number of actions to the right can vary between n (Schrödinger) to 0 (Heisenberg), giving $n+1$ possibilities. Besides the two limiting pictures (Schrödinger to Heisenberg) there are $n-1$ *intermediate* representations, in which the time dependence is shared by observables and phase-space density. Switching among representations is equivalent to carrying out an integration by parts. For computational purposes it is sometimes advantageous to work in one of these intermediate pictures.

There is no intermediate representation for the first order response function. For the second order response there is one intermediate representation,

$$S^{(2)}(t,\tau_2,\tau_1)=-\beta\frac{d}{d\tau_1}\langle\omega_{ij}B_k'(t)A_j'(\tau_2)M_{ik}^{(1)}(\tau_2,t)A(\tau_1)\rangle. \tag{33}$$

Note that while in the Heisenberg picture no time derivative appears in the second order response function, there is one in the intermediate picture and two in the Schrödinger picture.

In the case of the third order response function changing from the Schrödinger representation to the first intermediate representation reduces the highest order of stability matrices appearing in the equation by one [expressions include $M^{(1)}$ but not $M^{(2)}$]. We then get

$$\begin{aligned}S^{(3)}(t,\tau_3,\tau_2,\tau_1)=&-\beta^2\frac{d^2}{d\tau_1 d\tau_2}\langle\omega_{mn}B_l'(t)M_{ml}^1(\tau_3,t)\\ &\times A_n'(\tau_3)A(\tau_2)A(\tau_1)\rangle\\ &+\beta\frac{d}{d\tau_1}\langle\omega_{mn}B_l'(t)M_{ml}^1(\tau_3,t)A_n'(\tau_3)\\ &\times\omega_{ij}A_i'(\tau_2)A_k'(\tau_1)M_{jk}(\tau_2,\tau_1)\rangle.\end{aligned} \tag{34}$$

In contrast to the third order response function in the Schrödinger representation [see Eq. (21)], there are no second order stability matrices in the expression above. This significant computational advantage was exploited by Loring.[18] Naively, one might hope to get rid of even the first order stability matrix by proceeding another step towards the Heisenberg representation. When doing that, however, second order matrices return and one loses the numerical advantage.

IV. RESPONSE FUNCTIONS OF THE LORENTZ GAS

As an illustrative example, we have calculated the response of the Lorentz gas[19] to short pulses. This two-dimensional model consists of a point particle of mass m moving with momentum p through an infinite array of circular scatterers with radius R arranged on a triangular lattice with lattice constant a. To avoid difficulties in the calculation of stability matrices, the interaction energy $V(r)$ of the moving particle with the scatterers is assumed to be steep but smooth instead of impulsive. If the moving particle is farther away than R from the center of the scatterer, i.e., $r>R$, $V(r)=0$. For $r<R$ the interaction potential is given by $V(r)=\alpha(1-r^2)^4$ with $\alpha=10^{10}$ in all our numerical examples. At collisions with the scatterer the equations of motion of the system itself and of the stability matrices are integrated with the velocity Verlet algorithm.[20] The density of the scatterers $\rho\equiv N/V$ is related to the lattice constant by $\rho=2/(\sqrt{3}a^2)$. At close packing with the scatterer in contact $a=2R$ and the close packed density is $\rho=1/(2\sqrt{3}R^2)$. The state of the system is uniquely specified by coordinates and momenta, $x=\{x_0,x_1,x_2,x_3\}\equiv\{q_x,q_y,p_x,p_y\}$. Initial conditions of the moving particle are distributed canonically, i.e., positions $q\equiv\{q_x,q_y\}$ are homogeneously distributed in the area not occupied by the scatterers and momenta $p\equiv\{p_x,p_y\}$ are distributed according to $P(p)\propto\exp(-\beta p^2/2m)$. All results presented in this article were obtained for $\beta=1$. Throughout, the unit of length is R, the unit of energy is k_BT, the unit of momentum and field strength is $(mk_BT)^{1/2}$, and the unit of time is $(mR^2/k_BT)^{1/2}$.

We imagine that the Lorentz gas is perturbed at different times τ_i by short pulses $E_i\delta(t-\tau_i)$ coupling to q_x, the

x-coordinate of the moving particle. As a consequence of such an impulsive perturbation the x-component of the momentum, p_x, changes discontinuously from p_x to p_x+E_i. The resulting average current in x-direction, $j(t)\equiv\overline{p_x(t)}$, can be written in terms of the response functions $S^{(n)}(t,\tau_n,\ldots,\tau_1)$. For the Lorentz gas these response functions take particularly simple forms. For instance, the Schrödinger picture response functions up to order three are

$$S^{(1)}(t,\tau_1)=\left(\frac{\beta}{m}\right)\langle p_x(t)p_x(\tau_1)\rangle, \tag{35}$$

$$S^{(2)}(t,\tau_2,\tau_1)=\left(\frac{\beta}{m}\right)^2\langle p_x(t)p_x(\tau_2)p_x(\tau_1)\rangle - \left(\frac{\beta}{m}\right)\langle p_x(t)M_{22}^{(1)}(\tau_2,\tau_1)\rangle, \tag{36}$$

$$\begin{aligned}S^{(3)}(t,\tau_3,\tau_2,\tau_1)=&\left(\frac{\beta}{m}\right)^3\langle p_x(t)p_x(\tau_3)p_x(\tau_2)p_x(\tau_1)\rangle\\ &-\left(\frac{\beta}{m}\right)^2\langle p_x(t)p_x(\tau_1)M_{22}^{(1)}(\tau_3,\tau_2)\rangle\\ &-\left(\frac{\beta}{m}\right)^2\langle p_x(t)p_x(\tau_2)M_{22}^{(1)}(\tau_3,\tau_1)\rangle\\ &-\left(\frac{\beta}{m}\right)^2\langle p_x(t)p_x(\tau_3)M_{22}^{(1)}(\tau_2,\tau_1)\rangle\\ &+\left(\frac{\beta}{m}\right)\langle p_x(t)M_{k22}^{(2)}(\tau_2,\tau_2,\tau_1)\\ &\times M_{2k}^{(1)}(\tau_3,\tau_2)\rangle.\end{aligned} \tag{37}$$

Here, $M_{22}^{(1)}(\tau_2,\tau_1)\equiv\partial p_x(\tau_1)/\partial p_x(\tau_2)$ is a first order stability matrix element and $M_{k22}^{(2)}(\tau_2,\tau_2,\tau_1)\equiv\partial^2 p_x(\tau_1)/\partial x_k(\tau_2)\partial p_x(\tau_2)$ is a second order stability matrix element. In the above equation summation over the index k is implied.

We now apply the formalism developed in the preceding sections to the calculation of the response of the Lorentz gas to two short pulses with strengths E_1 and E_2 acting on the system at times τ_1 and τ_2, respectively. The resulting average current $j(t)$ is then measured at time t. In other words, we expose the system to the time dependent perturbation $E(t)=E_1\delta(t-\tau_1)+E_2\delta(t-\tau_2)$ and monitor the response of the system in terms of the nonequilibrium current $j(t,\tau_2,\tau_1)=j^{(1)}(t,\tau_2,\tau_1)+j^{(2)}(t,\tau_2,\tau_1)+j^{(3)}(t,\tau_2,\tau_1)+\cdots$ in different orders of the field. To first order the system responds linearly in the field strengths,

$$j^{(1)}(t,\tau_2,\tau_1)=E_1S^{(1)}(t,\tau_1)+E_2S^{(1)}(t,\tau_2). \tag{38}$$

While the second order response vanishes due by symmetry, the third order current is finite,

$$\begin{aligned}j^{(3)}(t,\tau_2,\tau_1)=\frac{1}{3!}\{&E_1^3S^{(3)}(t,\tau_1,\tau_1,\tau_1)+3E_1^2E_2\\ &\times S^{(3)}(t,\tau_2,\tau_1,\tau_1)+3E_1E_2^2S^{(3)}\\ &\times(t,\tau_2,\tau_2,\tau_1)+E_2^3S^{(3)}(t,\tau_2,\tau_2,\tau_2)\}.\end{aligned} \tag{39}$$

The third order response functions appearing in the above equation can be expressed as

$$S^{(3)}(t,\tau_1,\tau_1,\tau_1)=\left(\frac{\beta}{m}\right)^3\langle p_x(t)p_x^3(\tau_1)\rangle - 3\left(\frac{\beta}{m}\right)^2\langle p_x(t)p_x(\tau_1)\rangle, \tag{40}$$

$$\begin{aligned}S^{(3)}(t,\tau_2,\tau_1,\tau_1)=&\left(\frac{\beta}{m}\right)^3\langle p_x(t)p_x(\tau_2)p_x^2(\tau_1)\rangle\\ &-2\left(\frac{\beta}{m}\right)^2\langle p_x(t)M_{22}^{(1)}(\tau_2,\tau_1)p_x(\tau_1)\rangle\\ &-\left(\frac{\beta}{m}\right)^2\langle p_x(t)p_x(\tau_2)\rangle,\end{aligned} \tag{41}$$

$$\begin{aligned}S^{(3)}(t,\tau_2,\tau_2,\tau_1)=&\left(\frac{\beta}{m}\right)^3\langle p_x(t)p_x^2(\tau_2)p_x(\tau_1)\rangle\\ &-2\left(\frac{\beta}{m}\right)^2\langle p_x(t)p_x(\tau_2)M_{22}^{(1)}(\tau_2,\tau_1)\rangle\\ &-\left(\frac{\beta}{m}\right)^3\langle p_x(t)p_x(\tau_1)\rangle\\ &+\left(\frac{\beta}{m}\right)\langle p_x(t)M_{222}^{(2)}(\tau_2,\tau_2,\tau_1)\rangle,\end{aligned} \tag{42}$$

$$S^{(3)}(t,\tau_2,\tau_2,\tau_2)=\left(\frac{\beta}{m}\right)^3\langle p_x(t)p_x^3(\tau_2)\rangle - 3\left(\frac{\beta}{m}\right)^2\langle p_x(t)p_x(\tau_2)\rangle. \tag{43}$$

Most terms in the above equations are simple two and three time correlation functions of the momentum in x-direction and can be easily evaluated in an equilibrium molecular dynamics simulation. The evaluation of the terms depending on first and second order stability matrices, however, is numerically challenging. The reason for this difficulty lies in the fact the stability matrix elements grow exponentially in time due to the chaoticity of the underlying dynamics. As a consequence, averages involving stability matrices converge very slowly.

To illustrate this behavior we have calculated $\langle p_x(t)M_{22}^{(1)}(\tau_2,\tau_1)p_x(\tau_1)\rangle$, $\langle p_x(t)p_x(\tau_2)M_{22}^{(1)}(\tau_2,\tau_1)\rangle$, and $\langle p_x(t)M_{222}^{(2)}(\tau_2,\tau_2,\tau_1)\rangle$ for the Lorentz gas from an equilibrium simulation. Results for a density of $\rho=0.1R^{-2}$ are depicted in Fig. 1. While the expressions involving first order stability matrices can be accurately evaluated for times up to $t_2\approx 1.0$, $\langle p_x(t)M_{222}^{(2)}(\tau_2,\tau_1)\rangle$ is accurate only for very short times due to the extremely fast growth of the second order stability matrix. The growth of the first and second order stability matrix elements $M_{22}^{(1)}(\tau_2,\tau_1)$ and $M_{222}^{(2)}(\tau_2,\tau_2,\tau_1)$ with time is plotted in Fig. 2 for different densities. It is evident that the chaotic nature of the dynamics prevents us from calculating third order response functions in the Schrödinger picture even in a model as simple as the Lorentz gas,

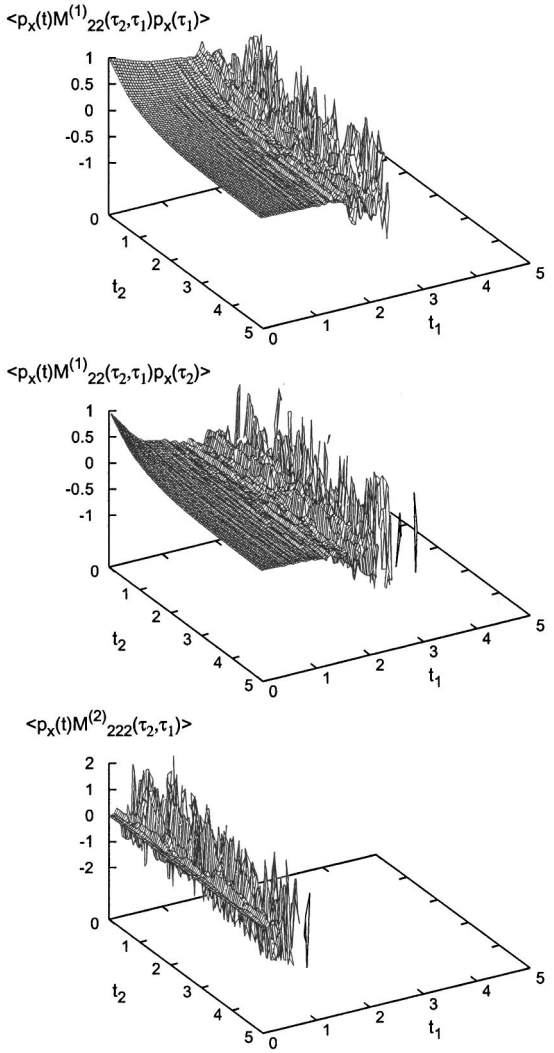

FIG. 1. The functions $\langle p_x(t)M_{22}^{(1)}(\tau_2,\tau_1)p_x(\tau_1)\rangle$, $\langle p_x(t)p_x(\tau_2)M_{22}^{(1)}\times(\tau_2,\tau_1)\rangle$, and $\langle p_x(t)M_{222}^{(2)}(\tau_2,\tau_1)\rangle$ (from top to bottom) as a function of the time intervals $t_2\equiv t-\tau_2$ and $t_1\equiv\tau_2-\tau_1$ for the Lorentz gas at a density of $\rho=0.10R^{-2}$. The results were obtained from 10^6 trajectories of length $t=10(mR^2/k_BT)^{1/2}$. While for short times t_1 the calculated surfaces are smooth, the exponentially growing stability matrix elements prevent an accurate calculations of the functions for larger times. This numerical errors is evident in the increased ruggedness of the surfaces with increasing t_1. The effect is particularly drastic for $\langle p_x(t)M_{222}^{(2)}(\tau_2,\tau_1)\rangle$ which cannot be evaluated even for time intervals t_1 much shorter than the average collision time which is $2.74(mR^2/k_BT)^{1/2}$ in this particular case.

for which we can integrate the equations of motion numerically at very low computational cost.

By changing from the Schrödinger to the first intermediate picture, one reduces the highest stability matrix order by one obtaining more benign expression for the third order response functions,

$$S^{(3)}(t,\tau_2,\tau_1,\tau_1)=\left(\frac{\beta}{m}\right)^2\langle p_x^2(\tau_1)M_{22}^{(1)}(\tau_2,t)\rangle - \left(\frac{\beta}{m}\right)^2\langle p_x(\tau_2)p_x(t)\rangle, \tag{44}$$

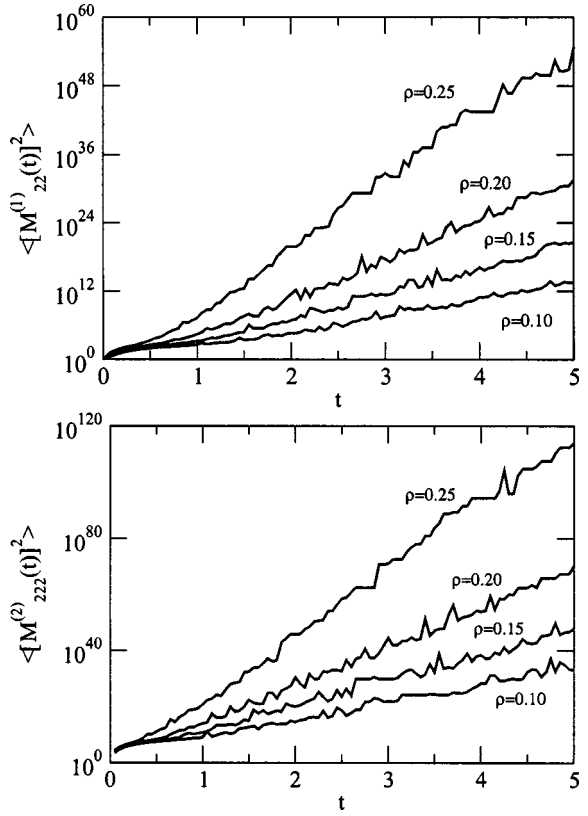

FIG. 2. Average of the squared stability matrix elements $M_{22}^{(1)}(t=\tau_2-\tau_1)$ (top) and $M_{222}^{(2)}(t=\tau_2-\tau_1)$ (bottom) as function of $t\equiv\tau_2-\tau_1$ for the Lorentz gas at different densities ρ.

$$S^{(3)}(t,\tau_2,\tau_2,\tau_1)=\left(\frac{\beta}{m}\right)^2\langle p_x(\tau_1)p_x(\tau_2)M_{22}^{(1)}(\tau_2,t)\rangle - \left(\frac{\beta}{m}\right)\langle M_{22}^{(1)}(\tau_2,\tau_1)M_{22}^{(1)}(\tau_2,t)\rangle. \tag{45}$$

Note that in these expressions no second order stability matrix appears. Instead, we have to average over a product of two first order stability matrices.

Results obtained in this intermediate picture are shown in Fig. 3. The function $\langle M_{22}^{(1)}(\tau_2,\tau_1)M_{22}^{(1)}(\tau_2,t)\rangle$ is shown in the top panel. The complete third order response $j^{(3)}(t,\tau_2,\tau_1)$ for the case $E_1=E_2=1.0(mk_BT)^{1/2}$ is depicted in the bottom panel. While in the intermediate picture one can calculate the third order response to longer time than in the Schrödinger picture, the chaoticity of the underlying dynamics still imposes strong bounds on the accuracy of the simulation in the long time regime. Nonequilibrium simulation techniques offer a way out of this limitation as will be discussed in Sec. VI.

If the dynamics of the system is regular, stability matrices grow slowly and response functions can be calculated even in the Schrödinger picture. To demonstrate this we have calculated the third order response for a quartic oscillator, i.e., a two-dimensional particle of mass m oscillating in a potential of the form $V(r)=\gamma r^4$, where r is the distance of the particle from the origin. Like in the Lorentz gas we imagine that the perturbation couples to the x-coordinate of the

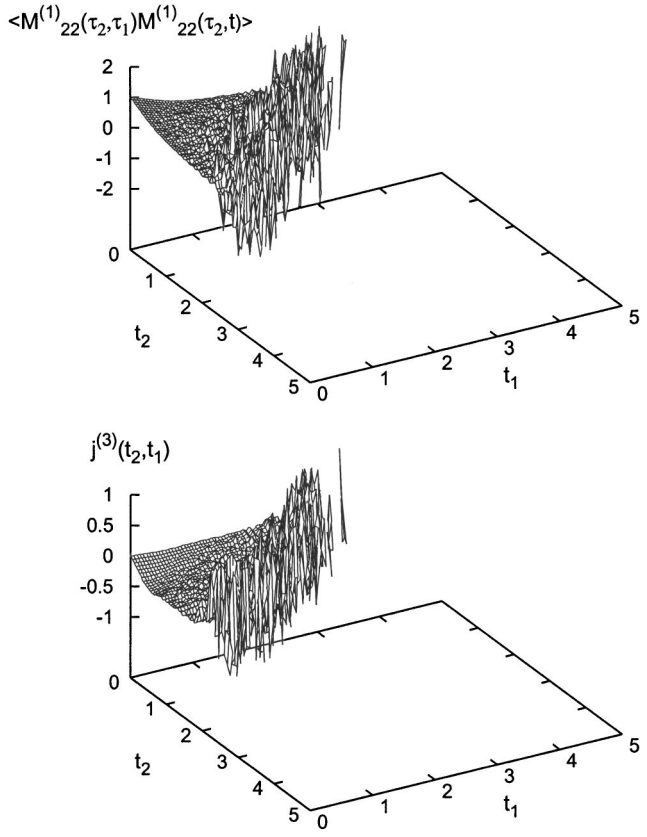

FIG. 3. Average $\langle M_{22}^{(1)}(\tau_2,\tau_1)M_{22}^{(2)}(\tau_2,t)\rangle$ and total third order response to two pulses with strengths $E_1=E_2=1.0(mk_BT)^{1/2}$ as a function of the time intervals t_1 and t_2 calculated for the Lorentz gas in the intermediate picture. Both plots were obtained for a density of $\rho=0.1R^{-2}$ from 10^6 trajectories of length $t=10(mR^2/k_BT)^{1/2}$. Evaluating the response functions in the intermediate picture mitigates the problems associated with the exponential growth of stability matrices, but does not eliminate them. In the example shown in the figure, the third order response can be accurately evaluated only for $t_1+t_2\approx 1.5(mR^2/k_BT)^{1/2}$. For longer times the numerical error becomes overwhelming.

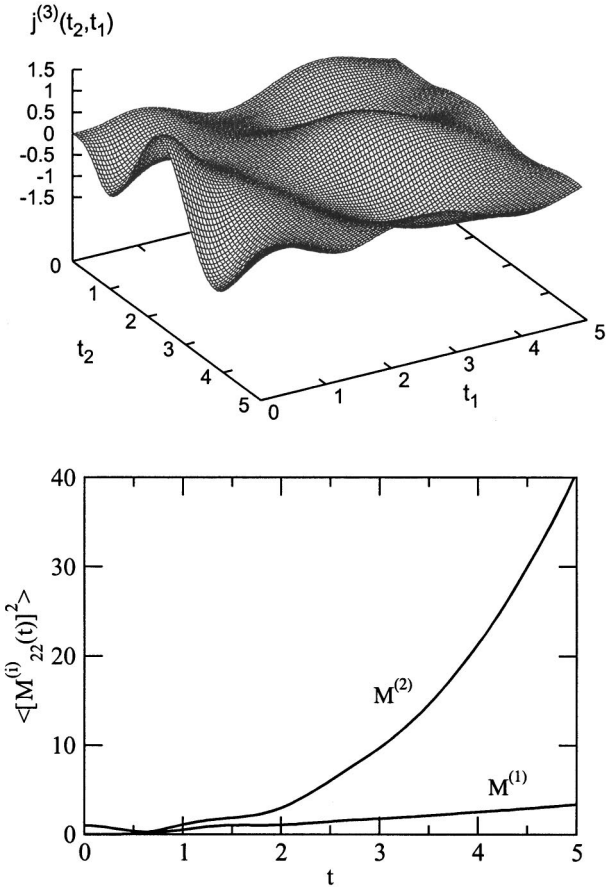

FIG. 4. (Top) total third order response to two pulses with strength $E_1=E_2=1.0(mk_BT)^{1/2}$ as a function of the time intervals t_1 and t_2 for the quartic oscillator described in the main text. The plot was obtained in the Schrödinger picture for a density of $\rho=0.1R^{-2}$ from 10^6 trajectories of length $t=10(mR^2/k_BT)^{1/2}$. (Bottom) average of the squared stability matrix elements $M_{22}^{(1)}(t=\tau_2-\tau_1)$ and $M_{222}^{(2)}(t=\tau_2-\tau_1)$ as a function of $t\equiv\tau_2-\tau_1$ for the quartic oscillator.

particle and that initial conditions are distributed canonically. We have calculated $j^{(3)}(t,\tau_2,\tau_1)$ for this model in the Schrödinger picture using Eqs. (39)–(43) and the results are depicted in Fig. 4 (here, $\gamma=1k_BT/R^4$). In the top panel the third order response is plotted as a function of the time delays $t_1\equiv\tau_2-\tau_1$ and $t_2\equiv t-\tau_2$. In contrast to the Lorentz gas, the surface is smooth indicating the absence of numerical problem associated with diverging stability matrices. This is evident also in the averaged square of the stability matrix elements $M^{(1)}$ and $M^{(2)}$ shown in the lower panel of Fig. 4. In contrast to the Lorentz gas, for which the stability matrix elements grow quickly to very large numbers, growth is modest in the quartic oscillator thus permitting the evaluation of averages involving stability matrices.

V. ONE-DIMENSIONAL RESPONSE TO A SINGLE INTENSE PULSE

Valuable insight into the nonlinear dynamics of the system can be gleaned from the response to a single short pulse perturbing the system at $t=0$. In this case, the nth order response function of the system is

$$S^{(n)}(t)=(-1)^n\int dxB(x)e^{-iLt}\{A,\ldots\{A,\rho\}\} \tag{46}$$

in the Schrödinger representation and

$$S^{(n)}(t)=\langle\{A\{\cdots\{A,B(t)\}\}\}\rangle \tag{47}$$

in the Heisenberg representation. The right-hand side of this equation (46) can be written as

$$\{A,\ldots\{A,\rho\}\}=\sum_{j=1}^{n}\beta^jC_j, \tag{48}$$

where the operators C_j are obtained by repeated applications of the Poisson bracket. Using Eq. (48) we can then recast Eq. (47) in the form

$$S^{(n)}(t)=\sum_{j=1}^{n}\beta^j\langle B(t)C_j\rangle. \tag{49}$$

The response functions to a single short perturbation become especially simple and easy to interpret if the observable A is one of the phase-space variables. So, assume that

$A=x_1$ and call this variable $q\equiv x_1$ and its conjugate momentum p. Then, the first few response functions in the Schrödinger picture are

$$S^{(1)}(t)=\left(\frac{\beta}{m}\right)\langle p(0)B(t)\rangle, \tag{50}$$

$$S^{(2)}(t)=\left(\frac{\beta}{m}\right)^2\langle p^2(0)B(t)\rangle-\left(\frac{\beta}{m}\right)\langle B(t)\rangle, \tag{51}$$

$$S^{(3)}(t)=\left(\frac{\beta}{m}\right)^3\langle p^3(0)B(t)\rangle-3\left(\frac{\beta}{m}\right)^2\langle p(0)B(t)\rangle, \tag{52}$$

$$S^{(4)}(t)=\left(\frac{\beta}{m}\right)^4\langle p^4(0)B(t)\rangle-6\left(\frac{\beta}{m}\right)^3\langle p^2(0)B(t)\rangle+3\left(\frac{\beta}{m}\right)^2\langle B(t)\rangle, \tag{53}$$

$$S^{(5)}(t)=\left(\frac{\beta}{m}\right)^5\langle p^5(0)B(t)\rangle-10\left(\frac{\beta}{m}\right)^4\langle p^3(0)B(t)\rangle+15\left(\frac{\beta}{m}\right)^3\langle p(0)B(t)\rangle. \tag{54}$$

In the Heisenberg picture the single pulse response function of order n is

$$S^{(n)}=\left\langle\frac{\partial^n p(t)}{\partial p^n(0)}\right\rangle=\langle M^{(n)}_{f,f}(t,0)\rangle, \tag{55}$$

where f is the dimension of configuration space. The partial derivatives in the above equation can be easily evaluated with the recursion formula,

$$\left\langle p^k(0)\frac{\partial^n p(t)}{\partial p^n(0)}\right\rangle=\left(\frac{\beta}{m}\right)\left\langle p^{k+1}(0)\frac{\partial^{n-1}p(t)}{\partial p^{n-1}(0)}\right\rangle-k\left\langle p^{k-1}(0)\frac{\partial^{n+1}p(t)}{\partial p^{n+1}(0)}\right\rangle. \tag{56}$$

Application of this recursion formula is equivalent to integration by parts and yields the time correlation function expressions obtained in the Schrödinger picture. In contrast to the multiple pulse case, stability matrices do not appear in the Schrödinger picture response functions for a single pulse. As a consequence, such response functions up to arbitrary order can be easily determined by calculating ordinary time correlation functions.

First, third, fifth, and seventh order response functions (from top to bottom) of the Lorentz gas as a function of time t and density ρ are depicted in Fig. 5. The first order response function $S^{(1)}(t)$ shown in the top panel is relatively smooth and featureless over the whole density range. At densities near close packing, however, $S^{(1)}(t)$ displays a slight negative dip originating from correlated collisions in the cage formed by the scatterers. At low densities, on the other hand, the first order correlation function decays exponentially. The higher order correlation functions $S^{(3)}(t)$, $S^{(5)}(t)$, and $S^{(7)}(t)$ acquire additional features in the high density range but remain smooth for low densities, at which collisions are uncorrelated. In fact, in the low density regime response

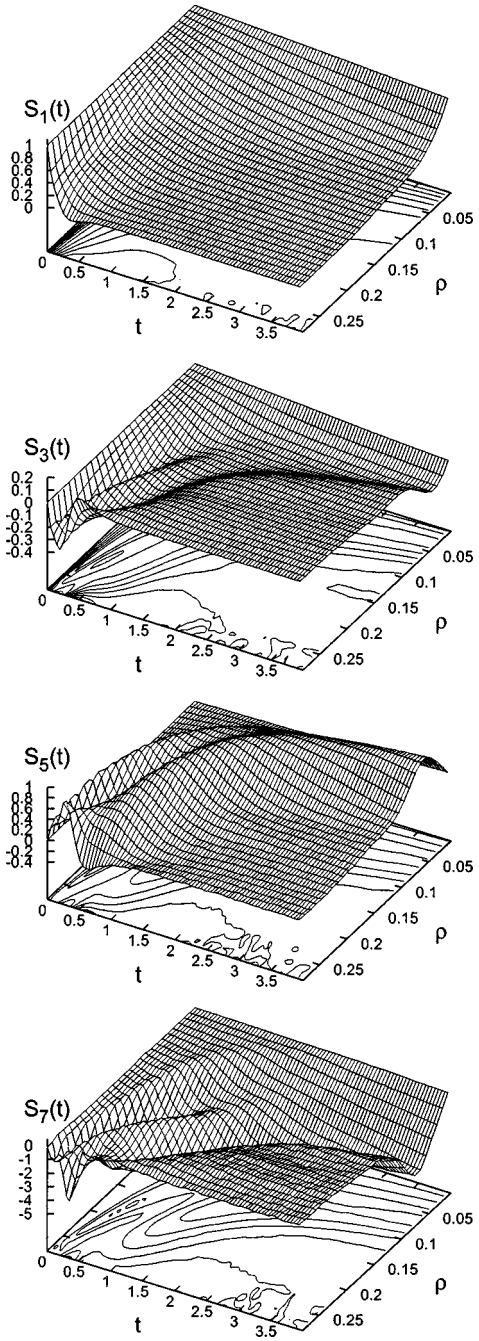

FIG. 5. First, third, fifth, and seventh order response functions (from top to bottom) of the Lorentz to a single pulse as a function of time t and density ρ.

functions for the Lorentz gas can be obtained analytically to arbitrary order from a simple model with exponential distribution of collision times.[21]

VI. NONEQUILIBRIUM, FINITE FIELD, SIMULATIONS

It is also possible to calculate NRFs using a nonequilibrium simulation strategy. In this approach which more closely mimics real experiments,[14] one applies finite perturbations to the system. For a sequence of impulsive perturbations the free time evolution of the system according to H_0 is punctuated by interactions with a finite field which causes

the system to jump discontinuously in phase-space. The corresponding nonequilibrium phase-space density evolves according to

$$\rho(t)=\mathcal{G}(t-\tau_n)\cdots\tilde{T}\mathcal{G}(\tau_2-\tau_1)\tilde{T}\rho_{\mathrm{equ}}, \tag{57}$$

where

$$\tilde{T}=\exp(-E\tilde{A}) \tag{58}$$

is the operator associated with the finite field perturbation. In a practical nonequilibrium simulation one generates initial conditions according to an equilibrium distribution, for instance, the canonical ensemble. Then, each of the initial conditions is evolved in time by integration of the appropriate equations of motion. At times τ_i this free evolution is interrupted and the system is displaced in phase-space in a way depending on both the strength of the external field and on how it couples to the system. After each perturbation the free evolution is resumed and carried out until the next interactions with the external field occurs. Finally, the value of the dynamical variable $B(t)$ is determined at time t. Averaging over a large number of such nonequilibrium trajectories yields $\langle B(t)\rangle$, the full response of the system to finite field perturbations. For each particular set of interaction times τ_i a separate simulation must be carried out. This is in contrast to equilibrium simulations in which response functions can be calculated for all times τ_i from a single long trajectory.

While in an equilibrium simulation the different orders of the system's response are calculated separately, a nonequilibrium simulations yields only the total response of the system, i.e., the sum of all orders. Equation (57) is a generating function for response functions. It represents coupling to fields that are short but not necessarily weak. To separate the different orders, simulations at different field strengths need to be carried out. For instance, the first order response can be extracted from a simulation carried out for small, but finite perturbations provided all higher orders can be neglected. Next, one increases the strengths of the perturbation to a level, where the second order becomes important, but all higher order responses are still negligible. The second order is then extracted by subtracting the linear response from the total response of the system. One can proceed in an analogous way to obtain higher order responses. Since the field strength at which a particular order becomes negligible is unknown *a priori*, this procedure requires some trial and error. More systematic approaches can be developed to separate different response orders from simulations carried out for different field strengths.[21]

As an example for a nonequilibrium simulation, we have calculated the average nonequilibrium current $j(t,\tau_2,\tau_1)$ at time t induced by two impulsive perturbations with field strengths E_1 and E_2 acting on the Lorentz gas described in the previous sections at times τ_1 and τ_2, respectively. Again, the distribution of initial conditions is canonical and the external field couples to the x-coordinate of the moving particle. Each time the external field acts on the system, the momentum of the moving particle is changed from p_x to p_x+E. The nonequilibrium current $j(t)$ is then obtained by averaging $p_x(t)$ over many nonequilibrium trajectories. Assuming that response orders higher than three are negligible,

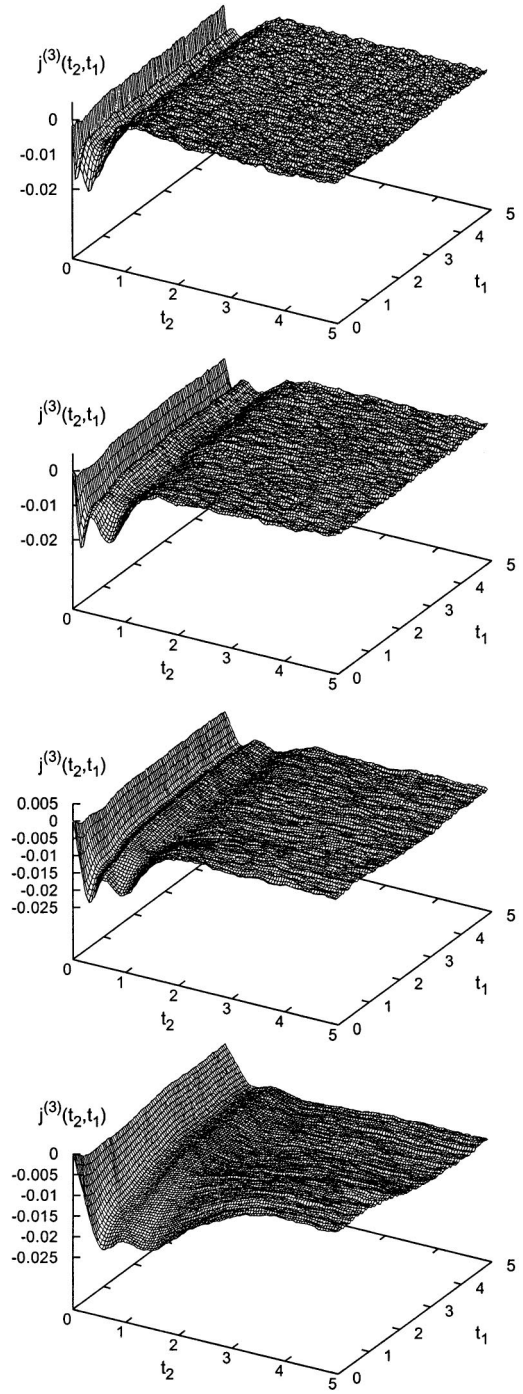

FIG. 6. Third order response $j^{(3)}$ as a function of the time intervals t_1 and t_2 for densities $\rho=0.25R^{-2}$, $\rho=0.20R^{-2}$, $\rho=0.15R^{-2}$, and $\rho=0.10R^{-2}$ (from top to bottom) and field strengths $E_1=E_2=0.4(mk_BT)^{1/2}$. Each surface was obtained from a nonequilibrium simulation of 20×10^6 trajectories of length $t=10(mR^2/k_BT)^{1/2}$ each.

we can obtain the third order response by subtracting the linear response $j^{(1)}(t)$ [see Eq. (38)] from $j(t)$, the total response of the system. In this particular case we used the linear response obtained from a separated equilibrium simulation. Third order responses obtained for the densities $\rho=0.25R^{-2}$, $\rho=0.20R^{-2}$, $\rho=0.15R^{-2}$, and $\rho=0.10R^{-2}$ (from top to bottom) and field strengths $E_1=E_2=0.4(mk_BT)^{1/2}$ are shown in Fig. 6. At all densities, the third order response can be determined accurately for all times

considered. This is in contrast to the equilibrium results discussed in the previous sections, which for longer times were strongly limited in accuracy by the Lyapunov instability of the underlying dynamics.

To extract response functions $S^{(n)}$ rather then responses $j^{(n)}$ from nonequilibrium data, several simulations for different field strengths E_i need to be carried out. For instance, one might be interested in knowing the response functions $S^{(3)}(t,\tau_1,\tau_1,\tau_1)$, $S^{(3)}(t,\tau_2,\tau_1,\tau_1)$, $S^{(3)}(t,\tau_2,\tau_2,\tau_1)$, and $S^{(3)}(t,\tau_2,\tau_2,\tau_2)$ appearing in Eq. (39). While $S^{(3)}(t,\tau_1,\tau_1,\tau_1)$ and $S^{(3)}(t,\tau_2,\tau_2,\tau_2)$ are best calculated from equilibrium simulations (expressions for single pulse response functions can be written without stability matrices), calculation of $S^{(3)}(t,\tau_2,\tau_1,\tau_1)$ and $S^{(3)}(t,\tau_2,\tau_2,\tau_1)$ requires two nonequilibrium simulations carried out for different combinations of field strengths E_1 and E_2 (for example, $E_1=E_2$ and $E_1=-E_2$).

VII. DISCUSSION

Correlation functions are given by moments of joint distribution functions of the relevant variable obtained by successive measurements. Let us consider for example an operator $A(q)$ that depends solely on coordinates but not on the momenta. $n+1$ measurements of the coordinate yield the joint distribution $T^{(n+1)}(q_{n+1}\tau_{n+1},\ldots,q_1\tau_1)$ of measuring q_1 at τ_1, q_2 at τ_2, and so on. The $n+1$ point correlation function of A is then given by

$$\langle A(\tau_1)\cdots A(\tau_{n+1})\rangle = \int\cdots\int T^{(n+1)}(q_{n+1}\tau_{n+1},\ldots,q_1\tau_1) \times A(q_1)\cdots A(q_{n+1})dq_1\cdots dq_{n+1}. \tag{59}$$

Let us consider now an nth order response measurement involving A [Eq. (13) with $B=A$]. To represent $S^{(n)}$ we introduce the joint distribution in phase-space (coordinates and momenta) $H(x_{n+1}\tau_{n+1},\ldots,x_1\tau_1)$ where $x_j=q_jp_j$. Equation (13) can then be recast in the form[22]

$$S^{(n)}(\tau_{n+1}\cdots\tau_1) = \int\cdots\int dx_1\cdots dx_{n+1} \times F^{(n+1)}(x_{n+1}\tau_{n+1},\ldots,x_1\tau_1), \tag{60}$$

where $\tau_{n+1}=t$ and

$$F^{(n+1)}(x_{n+1}\tau_{n+1},\ldots,x_1\tau_1) = A(q_{n+1})A'(q_n)\cdots A'(q_1)\frac{\partial}{\partial p_n}\cdots\frac{\partial}{\partial p_1} \cdot H(x_{n+1}\tau_{n+1},\ldots,x_1\tau_1), \tag{61}$$

and $A'(q)\equiv\partial A/\partial q$. The correlation function depends on the joint distribution of coordinates $T^{(n+1)}$, whereas the response function requires the joint distribution in phase-space $F^{(n+1)}$. Note that

$$T^{(n+1)}(q_{n+1}\tau_{n+1},\ldots,q_1\tau_1) = \int\cdots\int dp_1\cdots dp_{n+1}F^{(n+1)}(x_{n+1}\tau_{n+1},\ldots,x_1\tau_1). \tag{62}$$

$T^{(n+1)}$ does not contain enough information to compute the response since the momenta were integrated out. Response functions thus carry more information than the corresponding correlation functions. The stability matrices provide the extra information required for computing the NRF. The fact that classical correlation functions do not carry enough information for computing the NRF has important practical implications for simulation strategies: It is not possible to simulate and interpret NRF as standard equilibrium fluctuations, since NRF contain additional nonequilibrium information.

The relative merits of equilibrium versus nonequilibrium (finite field) simulation algorithms can be rationalized as follows. Equilibrium expressions for nonlinear response functions can be easily derived in the Schrödinger, Heisenberg, or an intermediate picture. All these expressions involve stability matrices. Although stability matrices such as $M^{(1)}(\tau_1,\tau_2)$ can be determined in molecular dynamics simulations by solving an appropriate set of equations of motion, serious difficulties are encountered in the evaluation of averages involving stability matrices $M^{(i)}$. The reason is that due to the chaotic dynamics of nonlinear systems the matrix elements of stability matrices grow exponentially in time. Averaging over such diverging quantities leads to extremely slow convergence. This behavior practically forbids equilibrium calculation of such nonlinear response functions for time larger than the typical time scale of chaos. Changing between different representations can slightly ameliorate the problem, but does not solve it. Obtaining a numerically stable equilibrium simulation strategy not suffering from is an open challenge.

In the nonequilibrium approach the Lyapunov instability of the underlying dynamics has no similar deleterious effect. The response of the system is determined by averaging over many independent trajectories which are perturbed by finite external fields. For each specific sequence of perturbations such simulations need to be repeated. In addition, extracting NRFs from the finite field response requires several simulations carried out for different field strength. In contrast, equilibrium simulations yield (in principle) NRFs for all orders and times from a single simulated trajectory. The need for repeated simulations in the nonequilibrium approach causes extra computational cost. This cost is, however, compensated by the benefit of the absence of diverging quantities.

While the appearance of stability matrices in the equilibrium expressions for NRFs poses serious computational problems it also raises the hope that multidimensional nonlinear spectroscopy might be used to experimentally detect chaotic motion. We have demonstrated that the multidimensional nonlinear response of classical systems to a sequence of n short pulses contains valuable dynamical information that can be recast in terms of n point correlation functions and the nth order stability matrices $M^{(n)}$ which contain higher order generalized Lyapunov exponents. In general

$S^{(n)}$ depends on n point correlation functions as well as nth order stability matrices $M^{(n)}$. $M^{(1)}$ is commonly used in the study and characterization of chaotic systems (Lyapunov exponents). $M^{(n)}$, which has not been studied in detail, should contain a wealth of additional information. This is an open challenge for simulations.

ACKNOWLEDGMENTS

The support of the National Science Foundation Grant No. CHE-0132571 is gratefully acknowledged. The calculations were carried out on the Schrödinger Linux cluster of the Vienna University Computer Center.

[1] L. Onsager, Phys. Rev. **37**, 405 (1931); **38**, 2265 (1931).
[2] R. Kubo, Rep. Prog. Phys. **29**, 255 (1966).
[3] R. Zwanzig, *Nonequilibrium Statistical Mechanics* (Oxford University Press, Oxford, 2001).
[4] R. R. Ernst, G. Bodenhausen, and A. Wokaun, *Principles of Nuclear Magnetic Resonance in One and Two Dimensions* (Clarendon, Oxford, 1987).
[5] S. Mukamel, *Principles of Nonlinear Optical Spectroscopy* (Oxford University Press, New York, 1995).
[6] S. Mukamel and R. M. Hochstrasser, Chem. Phys. **266**, No. 2, 3 (2001) (Special Issue).
[7] *Ultrafast Phenomena XII*, edited by T. Elsaesser, S. Mukamel, M. Murnane, and N. Scherer (Springer-Verlag, Berlin, 2000).
[8] A. Ma and R. M. Stratt, Phys. Rev. Lett. **85**, 1004 (2000).
[9] R. A. Denny and D. R. Reichman, Phys. Rev. E **63**, 065101(R) (2001).
[10] J. Cao, S. Yang, and J. Wu, J. Chem. Phys. **116**, 3760 (2002); J. Cao, J. Wu, and S. Yang, *ibid.* **116**, 3739 (2002).
[11] S. Saito and I. Ohmine, Phys. Rev. Lett. **88**, 207401 (2002).
[12] S. Mukamel, V. Khidekel, and V. Chernyak, Phys. Rev. E **53**, R1 (1996).
[13] C. Dellago and S. Mukamel, Phys. Rev. E **67**, 035205 (2003).
[14] T. I. C. Jansen, J. G. Snijders, and K. Duppen, J. Chem. Phys. **114**, 10910 (2001).
[15] R. Kubo, J. Photogr. Sci. **12**, 570 (1957).
[16] I. Oppenheim, Prog. Theor. Phys. Suppl. **99**, 369 (1989).
[17] H. B. Callen and T. A. Welton, Phys. Rev. **83**, 34 (1951).
[18] R. B. Williams and R. F. Loring, J. Chem. Phys. **113**, 1932 (2000).
[19] J. Machta and R. Zwanzig, Phys. Rev. Lett. **50**, 1959 (1983).
[20] M. P. Allen and D. J. Tildesley, *Computer Simulation of Liquids* (Clarendon, Oxford, 1987).
[21] C. Dellago and S. Mukamel, Bull. Korean Chem. Soc. **24**, 1107 (2003).
[22] V. Khidekel, V. Chernyak, and S. Mukamel, *Femtochemistry*, edited by M. Chergui (World Scientific, Singapore, 1996), p. 507.